624 Vol. 36, No. 3 / March 2019 / Journal of the Optical Society of America B Research Article

Journal of the Optical Society of America B OPTICAL PHYSICS

Difference frequency generation of ultraviolet from x-ray pulses in opaque materials

E. Minerbi* and S. Shwartz

Physics Department and Institute for Nanotechnology, Bar Ilan University, Ramat Gan 5290002, Israel
**Corresponding author: eviatar00@gmail.com*

Received 14 November 2018; revised 14 January 2019; accepted 14 January 2019; posted 14 January 2019 (Doc. ID 351817); published 12 February 2019

We suggest a new approach for observing x-ray nonlinear wave mixing in opaque materials. We focus on difference frequency generation of ultraviolet radiation from two short x-ray pulses by measuring the depletion of the pumping pulses. Like other processes involving nonlinear interactions between x-rays and longer wavelengths, our method can lead to the development of a probe for spectroscopy of valence electrons at the atomic scale resolution. The two main advantages of the method we propose over the direct observation of the generated signal are the ability to probe the properties of materials at wavelengths where they are opaque and the higher predicted efficiency in the ultraviolet regime. We describe a possible experimental setup with realistic specifications optimized with respect to the characteristics of the input pulses. We expect that experimental observations of the effect will be feasible with the new emerging high-repetition-rate x-ray free-electron lasers.

https://doi.org/10.1364/JOSAB.36.000624

1. INTRODUCTION

Although nonlinear processes at optical frequencies were first demonstrated more than 50 years ago [1–3], nonlinear light–matter interactions at x-ray wavelengths were hardly explored until recently. These interactions were indeed described nearly half a century ago by Freund and colleagues [4], and by Eisenberger and colleagues [5]. However, with earlier hard x-ray sources such as x-ray tubes and synchrotrons, experimental observations of nonlinear effects have been confined to the spontaneous processes of x-ray parametric down-conversion (PDC) [6–11]. We note that several pertinent effects such as third harmonic generation [12] and self-action effects [13] were analyzed theoretically.

In addition to being almost unexplored, nonlinear interactions between x-rays and longer wavelengths can lead to a method for probing the microscopic structure of chemical bonds and the density of valence electrons with the atomic scale resolution [5,9,14,15].

The new x-ray free-electron lasers (XFELs) producing femtosecond pulses of high brightness and peak intensity [16,17] make possible further novel experiments exploring nonlinear effects with x-rays. For example, x-ray and optical sum-frequency generation (SFG) in a diamond crystal was performed by Glover *et al.* [14]. X-ray second harmonic generation (SHG) in a diamond was observed by Shwartz *et al.* [18]. The efficiencies of those effects, though, are extremely small, no more than 10^{-7}. Higher-order nonlinear processes are orders of magnitude less efficient. For example, Tamasaku and colleagues reported the observation of x-ray two-photon absorption (TPA) in germanium with an efficiency of $\sim 10^{-13}$ [19], and in metallic copper [20]. X-ray TPA in zirconium was observed by Ghimire and colleagues *et al.* [21].

In difference frequency generation (DFG) of ultraviolet (UV) or visible pulses from two x-ray pulses, the frequency of the generated wave is equal to the difference of the two input frequencies. The DFG of optical radiation from two x-ray pump beams has been recently analyzed theoretically [22]. The approach considered in that work, which predicted an efficiency of 10^{-4}, is to directly measure the generated beam, while assuming that the pump is undepleted [22]. However, it is clear that such an approach is not applicable for materials that are opaque at the photon energy of the generated signal. This restriction limits the applicability of model to a very narrow range of wavelengths and materials. In addition, the measurement of the generated signal requires a careful design that can overcome the strong fluorescence noise in the optical regime, which is originated from the absorption of the x-ray pulses.

Here we extend the previous work on DFG to optically opaque materials. We show that it is possible to evaluate the efficiency of DFG by measuring the depletion of the x-ray pulses rather than the direct measurement of the intensity of the generated signal. This approach can overcome the challenges described above and opens the possibility to use DFG for spectroscopy of opaque materials. We estimate the pulse

energy loss of the pump beam due to the DFG process and predict that for two pump beams with a photon flux of 10^{11} photons/pulse, which can be achieved with available XFELs [23–25], the efficiency of the energy depletion of the pump beam that results from the DFG process can exceed 10^{-4}.

2. MODEL

We begin by describing the theoretical model, which is similar to the model that has been used to describe the DFG of x-rays into the optical regime where the material is transparent [22]. The main differences are the addition of the absorption to the generated wave and, since we propose to measure the depletion of the pump beam, we also include the depletion in the calculations, which is in contrast to our previous work [22]. The propagation of the waves in a nonlinear medium is described by the wave equation with a nonlinear term, which is given by

$$\nabla^2\vec{E} = \mu_0\left(\frac{\partial\vec{J}^{\mathrm{NL}}}{\partial t} + \epsilon_0\frac{\partial^2\vec{E}}{\partial t^2} + \epsilon_0\chi^{(1)}\frac{\partial^2\vec{E}}{\partial t^2}\right), \tag{1}$$

where $\vec{E}(\vec{r},t)$ is the electric field, μ_0 is the vacuum permeability, ϵ_0 is the vacuum permittivity, $\chi^{(1)}$ is the linear (first order) susceptibility, and $\vec{J}^{\mathrm{NL}}(\vec{r},t)$ is the nonlinear current density. We write the fields as $\vec{E}_{1,2,3}(\vec{r},t) = \frac{1}{2}E_{1,2,3}e^{i(\vec{k}_{1,2,3}\cdot\vec{r}-\omega_{1,2,3}t)}\hat{\epsilon}_{1,2,3} + \mathrm{c.c}$, where $E_{1,2,3}$ is the envelope function that varies slowly compared to the wave-number, k_i, and frequency, ω_i. $\hat{\epsilon}$ is the polarization vector of the field. With this simplification we can use the slowly varying envelope approximation (SVEA). This leads to coupled wave equations, which relate the pumping fields and the generated field envelopes, so

$$\begin{aligned}
&\frac{n_1}{c}\frac{\partial E_1}{\partial t} + \sin(\theta_1)\frac{\partial E_1}{\partial x} + \frac{\partial E_1}{\partial y} + \cos(\theta_1)\frac{\partial E_1}{\partial z} + \alpha_1 E_1 = \kappa E_2 E_3\\
&\frac{n_2}{c}\frac{\partial E_2}{\partial t} + \sin(\theta_2)\frac{\partial E_2}{\partial x} + \frac{\partial E_2}{\partial y} + \cos(\theta_2)\frac{\partial E_2}{\partial z} + \alpha_2 E_2 = \kappa E_1 E_3^*\\
&\frac{n_3}{c}\frac{\partial E_3}{\partial t} + \sin(\theta_3)\frac{\partial E_3}{\partial x} + \frac{\partial E_3}{\partial y} + \cos(\theta_3)\frac{\partial E_3}{\partial z} + \alpha_3 E_3 = \kappa E_1 E_2^*.
\end{aligned} \tag{2}$$

We denote E_1 and E_2 as the envelopes of the pumping beams and E_3 as the envelope of the generated beam. n_i is the refractive index, c is the speed of light in vacuum, α_i is the absorption coefficient, and κ is the nonlinear coefficient. θ_1, θ_2 are the propagation angles of the pump beams, and θ_3 is the propagation angle of the generated beam with respect to the normal to the crystal surface (see Fig. 1). The angles are determined by the phase-matching condition $\vec{k}_3 + \vec{G} = \vec{k}_1 - \vec{k}_2$. The phase matching is achieved using the reciprocal lattice vector. This is possible because wave vectors in the x-ray region are of the same order of magnitude as the reciprocal lattice vector. When a perfect phase matching is fulfilled, the individual atomic dipoles that constitute the material are properly phased. The field emitted by each dipole adds coherently in the propagating direction and the generated wave extracts energy most efficiently from the pumping waves. We note that the coupled equations shown in Eq. (2) include the conditions for phase matching and are correct as long as the wave envelopes vary slowly with respect to the UV period and wavelength, and the condition that the absorption length of each of the waves is much smaller than the wavelength is satisfied for all waves.

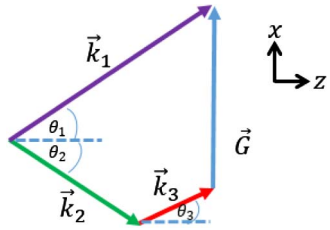

Fig. 1. Phase-matching scheme. $\vec{k}_1$, $\vec{k}_2$ and θ_1, θ_2 are the wave vectors and angles of propagation, respectively, of the pump pulses. $\vec{k}_3$ and θ_3 are the wave vector and angle of propagation, respectively, of the generated UV wave. $\vec{G}$ is the reciprocal lattice vector.

Equation (2) can be simplified by assuming that the depletion of the input waves is much smaller than their initial values, thus allowing us to write each wave as $E_i(x,y,z,t) = E_{i0}(x,y,z=0,t) + \delta E_i(x,y,z,t)$, where $\delta E_i \ll E_{i0}$, and solve the equations by keeping only the first order terms,

$$\begin{aligned}
&\frac{n_1}{c}\frac{\partial\delta E_1}{\partial t} + \sin(\theta_1)\frac{\partial\delta E_1}{\partial x} + \frac{\partial\delta E_1}{\partial y}\\
&\quad + \cos(\theta_1)\frac{\partial\delta E_1}{\partial z} + \alpha_1\delta E_1 = \kappa E_{20}\delta E_3\\
&\frac{n_2}{c}\frac{\partial\delta E_2}{\partial t} + \sin(\theta_2)\frac{\partial\delta E_2}{\partial x} + \frac{\partial\delta E_2}{\partial y}\\
&\quad + \cos(\theta_2)\frac{\partial\delta E_2}{\partial z} + \alpha_2\delta E_2 = \kappa E_{10}\delta E_3^*\\
&\frac{n_3}{c}\frac{\partial\delta E_3}{\partial t} + \sin(\theta_3)\frac{\partial\delta E_3}{\partial x} + \frac{\partial\delta E_3}{\partial y} + \cos(\theta_3)\frac{\partial\delta E_3}{\partial z} + \alpha_3\delta E_3\\
&= \kappa(E_{10}E_{20}^* + E_{10}\delta E_2^* + \delta E_1 E_{20}^*).
\end{aligned} \tag{3}$$

The nonlinear coefficient is related to the nonlinear current density by the following relation, $\kappa = \frac{\sqrt{2\hbar\eta_1\eta_2\eta_3\omega_1\omega_2\omega_3}J^{\mathrm{NL}}}{2\omega_3 E_1 E_2^*}$. We denote η_i as the impedance of the medium, and ω_i as the angular frequency. J^{NL} is the nonlinear current density that we estimate using the classical theoretical model for nonlinearity, and using the recently observed data of PDC into the optical regime, where we consider the nonlinearity coefficient as a fitting parameter.

In previous works the undepleted pump approximation was assumed. This assumption leads to a simplified model with no coupled equations that can be solved analytically [22]. Here, on the other hand, this simplification cannot be made inherently, since the depletion of the pump is the quantity we want to measure. Therefore, we need to solve the coupled equations shown in Eq. (3). These equations possess no analytical solution and are solved numerically. The theoretical value for the nonlinear current density is calculated in the same manner as in previous works, by using the classical model for x-ray and optical wave mixing [5,26]. The origin of the nonlinearity is the combination of three phenomena that include the Lorentz force, the perturbed charge density, and the Doppler shift

[5,10]. It was shown, that while those phenomena seem to be unrelated, they are all required to satisfy the detailed balance principle [27]. The nonlinear current, which is the source of E_3, the difference frequency generated wave, is defined by $\vec{J}^{(2)}_{\omega_3} = \rho^{(0)}\vec{v}^{(2)}_{\omega_3} + \rho^{(1)}_{\omega_1}\vec{v}^{(1)*}_{\omega_2} + \rho^{(1)*}_{\omega_2}\vec{v}^{(1)}_{\omega_1}$. To calculate the nonlinear current density, we use the classical equation of motion for a single electron that includes an effective restoring force and the electric and the Lorentz force, and the continuity equation [22,26]:

$$\frac{\partial^2\vec{r}}{\partial t^2} + (\vec{v}\cdot\nabla)\vec{v} + \omega_0^2\vec{r} = \frac{e}{m}(\vec{E} + \vec{v}\times\vec{B}), \tag{4}$$

$$\frac{\partial\rho}{\partial t} + \nabla\cdot(\rho\vec{v}) = 0. \tag{5}$$

Here, $\vec{r}$ is the electron displacement from its equilibrium position, $\vec{v}$ is the electron velocity, ρ is the charge density, m and e are the electron mass and charge, and ω_0 is the band-gap frequency [14]. $\vec{E}$ and $\vec{B}$ are the electric and magnetic fields of the beams, respectively. We solve Eqs. (4) and (5) by expanding the electron velocity and the charge density to the second order, as done in a previous work [22]. Since we are interested in the estimation of the effect for the calculation of the nonlinear current density we assume that the waves can be considered as monochromatic plane waves throughout the interaction. This is equivalent to the assumption that the nonlinear coefficient is constant in the photon energy range that we consider in Eq. (3), which is determined by the width of the input pulses. We then substitute the results in the definition of the second-order current density $\vec{J}^{(2)}_{\omega_3}$, as we described above. The dominant term of the nonlinear current density can be expressed as

$$\vec{J}^{(2)}_{\omega_3} = \frac{\rho_0 e^2}{4m}\left[\frac{\omega_3\cos(\theta_1+\theta_2)(\vec{k}_3+\vec{G})}{m\omega_1\omega_2(\omega_3^2-\omega_0^2)}\right]E_1E_2^*e^{i\Delta\vec{k}\cdot\vec{r}}, \tag{6}$$

where ρ_0 is the electron density in the absence of the pumping beam (electron density in uniform plasma), and $\vec{G}$ is the reciprocal lattice vector. E_i and $\vec{k}_i$ are the envelope and wave vector of the beam, oscillating at frequency ω_i. We note that this model agrees with the reported experimental results of interactions between x-rays and optical wavelengths when the optical wavelengths are below the band gap [14,28], but shows discrepancies when the photon energies of the long wavelengths are above the band gap [28]. The semi-empirical value for the nonlinear coupling coefficient is obtained by fitting the expression for the integrated count rate of PDC, including losses [11], to the experimental data described in Fig. 2 of [28].

We write the envelope of each of the fields as a transform-limited (TL) Gaussian,

$$E(x,y,z,t) = \sqrt{\frac{\left(\frac{2}{\pi}\right)^{1.5}N}{w_{x1,2}w_{y1,2}\tau_{1,2}\sec(\theta_{1,2})}}e^{-\left(\frac{x_{1,2}}{w_{x1,2}}\right)^2-\left(\frac{y}{w_{y1,2}}\right)^2-\left(\frac{t+\Delta\tau-z_{1,2}/v_{g1,2}}{\tau_{1,2}}\right)^2}, \tag{7}$$

where N is the number of photons per pulse, and $w_{x1,2}$ and $w_{y1,2}$ are the width of the waist of the beams in the $\hat{x}$ and $\hat{y}$ directions. $\tau_{1,2}$ is the pulse duration at the full width half maximum (FWHM), for each of the pulses, $\Delta\tau$ is the time delay between the two pulses, and v_g is the group velocity of the pump pulses. We define $x_{1,2} = x\cos\theta_{1,2} - z\sin\theta_{1,2}$ and $z_{1,2} = x\sin\theta_{1,2} + z\cos\theta_{1,2}$. We solve Eq. (3) together with the estimation of the nonlinear coupling coefficient as we described above, to find the electric fields of all waves. We obtain the figures below by integrating the solution of Eq. (3) for E_1 (the field of the first input beam) over the pulse duration and spatial coordinates perpendicular to the normal to the surface of the crystal (x, y).

3. NUMERICAL SIMULATIONS

To demonstrate the feasibility of the method we propose, we consider an example where two quasi-monochromatic pumping beams with center energies at 8.05 keV ($\lambda = 0.154$ nm) and 8.0435 keV ($\lambda = 0.15415$ nm) enter a diamond crystal at angles θ_1, θ_2 relative to the $\hat{z}$ direction and generate a wave with a center energy at 6.5 eV ($\lambda = 190$ nm), which propagates at an angle of θ_3, relative to the $\hat{z}$ direction (see Fig. 1). The reciprocal lattice vector normal to the C(111) atomic planes is used to fulfill the phase-matching condition. The phase-matching equations imply that the incident angles of the pumps are $\theta_1 = 21.856°$ and $\theta_2 = -22.103°$, and that the angle between the normal to the surface and the generated UV wave is $\theta_3 = 7.6°$. The pump input angles with respect to the atomic planes deviates from the Bragg angle by ~0.15°. The absorption coefficients and the refractive index for the x-ray pumps and for the generated UV were taken from tabulated data [29,30]. We consider two beams with equal waists.

We first consider the dependencies on the various properties of the pumping beams and identify the parameters that result in the maximum efficiency. We show our results in Fig. 2. The efficiency of the process is defined as the ratio between the number of the DFG photons and the number of incident pump photons. Since the generated beam is not directly measured, the number of generated photons is estimated as $N_{\mathrm{DFG}} = N_l - N_{nl}$, where N_l is the number of pump photons that are detected in the absence of the second beam (only linear absorption) and N_{nl} is the number of the pump photons that are detected when the second beam is present (linear absorption and the nonlinear process). The efficiency is therefore given by $\eta_{\mathrm{eff}} = (N_l - N_{nl})/N_{in}$, where N_{in} is the number of incident pump photons entering the nonlinear medium. We calculate the efficiency by calculating the number of photons per pulse of the pump with the nonlinear interaction and in its absence. This is obtained by integrating $E_1(x,y,z,t)^2$ over the time and the transverse directions of the propagation direction.

It is clear that the maximum efficiency is expected when phase matching is satisfied. However, it is also important to consider the dependence of the phase matching on the angular deviation from the perfect phase-matching angle. We plot the angular distribution of the DFG efficiency in Fig. 2(a). The width of this distribution is 0.8 mrad at full FWHM. As we will discuss below, this width is expected to be adequate for a practical setup.

Due to the weakness of the nonlinearity, intense focused pulses are required to achieve measurable efficiencies. However, as the beams are focused more tightly, their spatial

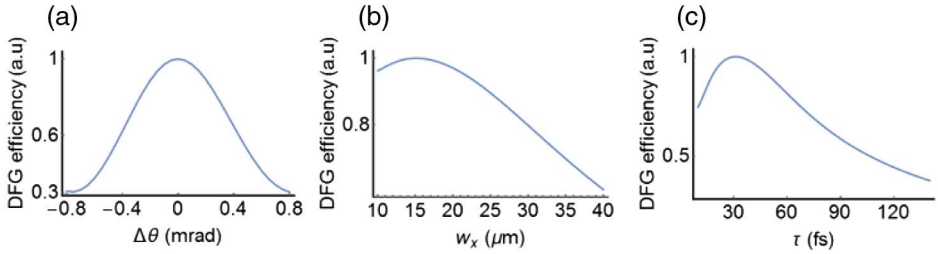

Fig. 2. Efficiency of the DFG process in arbitrary units as a function of (a) deviation from phase-matching angle, where the FWHM is 0.8 mrad. The pulse duration is 35 fs and the beam waist is 15 μm. (b) The beam width at phase matching and with pulse duration of 35 fs. (c) The duration of the pulses at phase matching with a beam waist of 15 μm.

overlap decreases since they propagate at different directions with an angle of $\theta_1 + \theta_2$ between them. Thus, there is a spatial walk-off and the interaction length is shorter [31]. Therefore, we expect to have a beam width, which leads to a maximal conversion efficiency as can be seen in Fig. 2(b). We find that the maximum DFG effect is observed for a beam width of 15 μm.

When examining the efficiency dependence on the pulse duration, the group velocity mismatch must also be considered. Since the two pumps propagate at different velocities, short pulses will suffer also from temporal walk-off. This effect contributes greatly for short pulses. However, we find that for pulse durations of 35 fs the dominant walk-off term is the spatial term, whereas for pulses shorter than 20 fs, the temporal term dominates [32,33]. We find that the maximum DFG effect is observed for a pulse duration of 35 fs, as can be seen in Fig. 2(c).

By introducing a delay between the two input pulses, we note that it is possible to get the temporal structure of the pulses. We therefore plot the dependence of the efficiency on the delay between the input pulses in Fig. 3. As expected, the most efficient wave mixing occurs when the delay approaches zero. We find that the FWHM is 70 fs. The distribution is slightly asymmetric because of the slightly different group velocities of the two pump beams.

After optimizing the pulses characteristics (duration, width, direction, and delay), we estimate the energy depletion of the pumping beams due to the nonlinear DFG process.

We note that the estimation of the efficiency is highly dependent on the estimation of the nonlinear coupling coefficient, which can only be estimated since there is no comprehensive theory for nonlinear interactions between x-rays and UV radiation in the range near the band-gap of the material. We therefore estimate the nonlinear susceptibility by fitting the

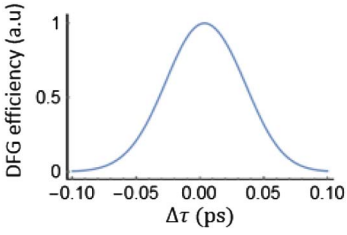

Fig. 3. Efficiency of the DFG process in arbitrary units as a function of the delay between the two x-ray pumps.

experimental data of the recently observed PDC of x-rays into the optical regime [28]. This procedure leads to a nonlinear susceptibility of $\chi^{(2)}_{(2,2,0)} = 2 \times 10^{-17}\ \frac{\mathrm{m}}{\mathrm{V}}$ and the corresponding DFG estimated efficiency for an input flux of 10^{11} photons per pulse is 1.5×10^{-4}. The calculation based on the classical model for nonlinearity, which has been used to describe the nonlinear interaction between x-rays and optical radiation [26], results in a nonlinear susceptibility of $2 \times 10^{-16}\ \frac{\mathrm{m}}{\mathrm{V}}$, and the efficiency for an input flux of 10^{11} photons per pulse is 10^{-2}. We note that this model agrees with the experimental results when the optical wave is at photon energies below the energy band gap, but shows discrepancies with the experimental results of PDC, for photon energies above the band gap [14,28].

We next address the ability to measure the effect with present-day technology. The ability to measure the depletion energy of the input beams depends on the ratio between the energy loss due to linear absorption and the energy depleted from the beam due to the nonlinear process. The pulses emerging from the SASE beam, however, do not have a Gaussian temporal shape but rather have the form of a sequence of spikes with stochastic phases and amplitudes. Therefore, we also estimate the depletion energy for temporally stochastic (TS) pulses in addition to the TL Gaussian pulses. These pulses resemble the temporal shape of the SASE beam [33]. As shown in [33], we describe the TS pulses as a chain of short Gaussian pulses with random phases,

$$E_{\mathrm{TS}}(x,y,z,t) = E(x,y,z,t) \times \sum_{m=-\infty}^{\infty} e^{i\phi_m} \times e^{-\left(\frac{t-m\Delta\tau_0 - z_{1,2}/v_{g1,2}}{\tau_0}\right)^2}, \tag{8}$$

where $E(x,y,z,t)$ is the TL Gaussian envelope given in Eq. (7). $\tau_0 = 2\sqrt{2\ \log(2)}\hbar/\Delta E$ is the minimal pulse duration, where ΔE, the FWHM of the power spectrum, was taken to be 1 eV. $\Delta\tau_0$ is the duration between adjacent spikes (taken to be $\Delta\tau_0 = \tau_0/5$), and ϕ_m is a randomly assigned phase.

In Fig. 4, we show the normalized pulse energy of one input beam as a function of the crystal length in the absence of the second beam (orange line) and when the second Gaussian beam (blue line) or TS beam (red dashed) is present. It is clear that the nonlinear effect is most pronounced when the energy transfer due to the nonlinear process is maximized at $z = 30$ μm. The length where the efficiency reaches its maximal value is determined by the overlap between the input beams. At this

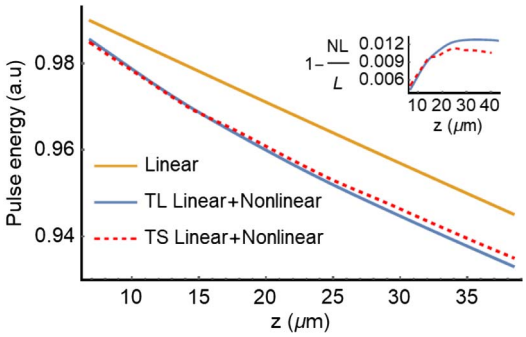

Fig. 4. Comparison between the pulse energy depletion of the pump with the nonlinear process (blue and dashed red) and in its absence, where the depletion is only due to the linear absorption (orange). Inset: ratio between the pulse energy depletion of the pump due to the linear absorption and the nonlinear process (NL), and the energy depletion of the pump due to linear absorption only (L) for TL Gaussian pulses (blue) and for TS pulses (red dashed). Pulse duration is 35 fs and the beam width is 15 μm. The depletion of the TS pulses is taken for an average over 7 pulses.

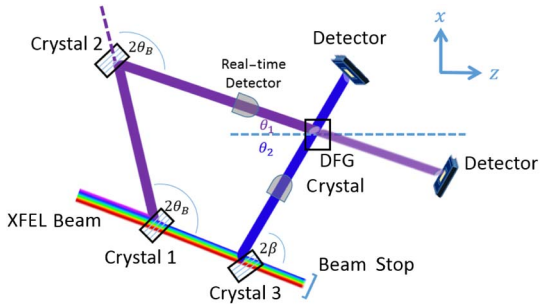

Fig. 5. Schematic of a possible experimental setup. A beam with a broad spectrum hits the first Bragg crystal. Crystal 1 and crystal 2 are tuned to the same Bragg angle and crystal 3 is tuned to the Bragg angle of the second wavelength. Crystal 4 is the crystal used for the DFG process. The detector measures the pulse energy after crystal 4. Real-time detectors are used to measure the pulse energies of the input beams before the nonlinear crystal. They can be implemented, for instance, using a thin foil that scatters a small portion of the intensity into a photodiode.

distance the ratio between the pulse energy loss due to the nonlinearity and the pulse energy loss without the nonlinearity (linear absorption) is the largest and is equal to 1.2×10^{-2} when a TL Gaussian beam is assumed (1×10^{-2} for a TS beam). Since we propose to use a monochromator, which restricts the bandwidth of the input beams at the nonlinear crystal, the difference between the spectra of the TL Gaussian pulses and the TS pulses are smaller than without the monochromator. In addition, an average over a large number of these TS pulses results with the assumed TL Gaussian pulse shape [33,34]. Therefore, the energy depletions of the two pulses are comparable. The small deviation between them is due to the nonlinear characteristics of the interaction, which becomes more pronounced at larger propagation distances.

4. SUGGESTED EXPERIMENTAL SETUP

To complete our proposal for the measurement of the depletion of the pulse energy of the input beams as a means to measure the nonlinear effect of DFG of UV pulses from two x-ray pulses, we describe a possible experimental setup. The two quasi-monochromatic pump beams must satisfy the phase-matching condition. Consequently, the angle between the two beams is nearly equal to twice the Bragg angle. This requirement can be fulfilled by the arrangement of crystals described in Fig. 5. All the crystals in this example are diamond crystals, where we use the same reflection (in this example we use the C(111) reflection). The input beam is the broad-spectrum self-amplified spontaneous emitted (SASE) beam. Crystal 1 and crystal 2 are tuned to the Bragg angle of the first beam (8.05 keV) at $\theta_B = 21.96°$. Crystal 1 reflects the beam in the direction of crystal 2, and crystal 2 reflects the first beam into the DFG crystal. Crystal 3 is tuned to the photon energy of the second beam at 8.0435 keV (the Bragg angle is $\beta = 21.98°$), and it reflects the second beam into the DFG crystal. With this setup, the angle between the two pump beams is $\theta_1 + \theta_2 = 43.96°$. Crystal 4 is the DFG crystal.

We note that the input SASE beam suffers from large pulse energy and spectral fluctuations. Since the proposed setup relies on the use of a Bragg beam splitter and reflectors similar to those that are used in current split and delay systems [35,36], the central photon energies of the input beams at the input of the nonlinear crystal are fixed but their intensities (and spectra) fluctuate stronger than the intensity of a SASE beam before the first crystal. Therefore, the comparison between the linear and the nonlinear depletion as shown in Fig. 4 requires very careful shot-to-shot measurements of the pulse energies and spectra of the input beams before and after the nonlinear crystal. Real-time detectors can be used to measure the quantities of the input beam using a thin foil that scatters a small portion of the intensity into a photodiode. The uncertainty in the pulse intensity due to the strong SASE fluctuations is linearly dependent on the intensity. Therefore, the variation of the pulse intensity will not affect the pulse detection statistics. We conclude that counting statistics is the main source for errors that cannot be eliminated. Current detectors can measure the number of photons per pulse with an absolute uncertainty of <10% [37–39]. Hence, about 10^6 pulses are required to obtain a standard error of 10^{-4}, which is sufficient to differentiate the nonlinear depletion according to our stringent estimation of the effect, from the linear depletion. Consequently, the measurement of the effect is expected to gain significantly using high-repetition-rate FELs. For example, using the European XFEL, which can deliver 2.7×10^4 pulses per second, the measurement time is expected to be ~40 seconds; using LCLS II, where the number of pulses per second will be $\sim 10^6$, the measurement time will be only a few seconds [40–44]. We also note that the nonlinear depletion depends on the intensity of the input beam; therefore, a more intense source will require less repetitions to differentiate the two effects. The dependence of the depletion originating from the DFG effect is expected to vary linearly with the pump intensities, in contrast to the efficiencies of linear depletion processes, which are independent of the intensities. Therefore, measuring this dependence indicates that the depletion is

due to DFG and can be used to distinguish the effect from other effects. In addition, it is also possible to discriminate the DFG from other effects that are not wave mixing by blocking one of the beams, since the DFG effect should vanish with only one beam. Another possible mechanism to estimate the absorption is by detecting the fluorescence. However, in diamond for example, only the visible wavelengths will be detected while the UV wavelengths will be absorbed.

5. SUMMARY AND CONCLUSIONS

In conclusion, we considered a new approach to measure the nonlinear mixing of x-rays and longer wavelengths by measuring the depletion of the pumping pulses. We then analyzed the effect of the DFG of ultraviolet radiation from two short x-ray pulses. This method opens the possibility to measure DFG in the x-ray regime with various materials, including materials that are opaque at the generated signal wavelength. Our work predicts efficiencies that are higher than x-ray and visible wave mixing, which we relate to the resonant enhancement of the nonlinearity near the binding energies of the valence electrons in the sample. Despite the resonant enhancement, our calculations indicate that the measurement of the effect requires high-repletion-rate XFELs.

Finally, the method we propose advances the possibility to use x-ray nonlinear interactions as a probe for valence electron spectroscopy at the atomic scale resolution. The nonlinear current density, which drives the nonlinear process, is related to the atomic charge density, as can be seen from Eq. (6). Hence, it is possible to reconstruct the valence electron charge distribution using a series of measurements of the Fourier components of the nonlinear susceptibility [9]. Because it is possible to control the delay between the input pulses, we believe our method can lead to the development of a probe for the dynamics of events associated with the charge distribution of valence electrons with temporal resolution of sub-femtoseconds.

Funding. Israel Science Foundation (ISF) (201/17).

REFERENCES

1. P. A. Franken, A. E. Hill, C. W. Peters, and G. Weinreich, "Generation of optical harmonics," Phys. Rev. Lett. **7**, 118–119 (1961).
2. M. Bass, P. A. Franken, A. E. Hill, C. W. Peters, and G. Weinreich, "Optical Mixing," Phys. Rev. Lett. **8**, 18 (1962).
3. A. W. Smith and N. Braslau, "Observation of an optical difference frequency," J. Appl. Phys. **34**, 2105–2106 (1963).
4. I. Freund and B. F. Levine, "Optically modulated x-ray diffraction," Phys. Rev. Lett. **25**, 1241–1245 (1970).
5. P. Eisenberger and S. L. McCall, "X-ray parametric conversion," Phys. Rev. Lett. **26**, 684–688 (1971).
6. H. Danino and I. Freund, "Parametric down conversion of x rays into the extreme ultraviolet," Phys. Rev. Lett. **46**, 1127–1130 (1981).
7. Y. Yoda, T. Suzuki, X.-W. Zhang, K. Hirano, and S. Kikuta, "X-ray parametric scattering by a diamond crystal," J. Synchrotron Radiat. **5**, 980–982 (1998).
8. B. Adams, P. Fernandez, W.-K. Lee, G. Materlik, D. M. Mills, and D. V. Novikov, "Parametric down conversion of x-ray photons," J. Synchrotron Radiat. **7**, 81–88 (2000).
9. K. Tamasaku, K. Sawada, E. Nishibori, and T. Ishikawa, "Visualizing the local optical response to extreme-ultraviolet radiation with a resolution of I λ/380," Nat. Phys. **7**, 705–708 (2011).
10. K. Tamasaku, K. Sawada, and T. Ishikawa, "Determining x-ray nonlinear susceptibility of diamond by the optical Fano effect," Phys. Rev. Lett. **103**, 254801 (2009).
11. S. Shwartz, R. N. Coffee, J. M. Feldkamp, Y. Feng, J. B. Hastings, G. Y. Yin, and S. E. Harris, "X-ray parametric down-conversion in the Langevin regime," Phys. Rev. Lett. **109**, 013602 (2012).
12. P. L. Shkolnikov and A. E. Kaplan, "X-ray third-harmonic generation in plasmas of alkalilike ions," Opt. Lett. **16**, 1973–1975 (1991).
13. P. L. Shkolnikov and A. E. Kaplan, "Feasibility of x-ray resonant nonlinear effects in plasmas," Opt. Lett. **16**, 1153–1155 (1991).
14. T. E. Glover, D. M. Fritz, M. Cammarata, T. K. Allison, S. Coh, J. M. Feldkamp, H. Lemke, D. Zhu, Y. Feng, R. N. Coffee, M. Fuchs, S. Ghimire, J. Chen, S. Shwartz, D. A. Reis, S. E. Harris, and J. B. Hastings, "X-ray and optical wave mixing," Nature **488**, 603–608 (2012).
15. U. Harbola and S. Mukamel, "Coherent stimulated x-ray Raman spectroscopy: attosecond extension of resonant inelastic x-ray Raman scattering," Phys. Rev. B **79**, 085108 (2009).
16. P. Emma, R. Akre, J. Arthur, R. Bionta, C. Bostedt, J. Bozek, A. Brachmann, P. Bucksbaum, R. Coffee, F.-J. Decker, Y. Ding, D. Dowell, S. Edstrom, A. Fisher, J. Frisch, S. Gilevich, J. Hastings, G. Hays, P. Hering, Z. Huang, R. Iverson, H. Loos, M. Messerschmidt, A. Miahnahri, S. Moeller, H.-D. Nuhn, G. Pile, D. Ratner, J. Rzepiela, D. Schultz, T. Smith, P. Stefan, H. Tompkins, J. Turner, J. Welch, W. White, J. Wu, G. Yocky, and J. Galayda, "First lasing and operation of an ångstrom-wavelength free-electron laser," Nat. Photonics **4**, 641–647 (2010).
17. B. W. J. McNeil and N. R. Thompson, "X-ray free-electron lasers," Nat. Photonics **4**, 814–821 (2010).
18. S. Shwartz, M. Fuchs, J. B. Hastings, Y. Inubushi, T. Ishikawa, T. Katayama, D. A. Reis, T. Sato, K. Tono, M. Yabashi, S. Yudovich, and S. E. Harris, "X-ray second harmonic generation," Phys. Rev. Lett. **112**, 163901 (2014).
19. K. Tamasaku, E. Shigemasa, Y. Inubushi, T. Katayama, K. Sawada, H. Yumoto, H. Ohashi, H. Mimura, M. Yabashi, K. Yamauchi, and T. Ishikawa, "X-ray two-photon absorption competing against single and sequential multiphoton processes," Nat. Photonics **8**, 313–316 (2014).
20. K. Tamasaku, E. Shigemasa, Y. Inubushi, I. Inoue, T. Osaka, T. Katayama, M. Yabashi, A. Koide, T. Yokoyama, and T. Ishikawa, "Nonlinear spectroscopy with x-ray two-photon absorption in metallic copper," Phys. Rev. Lett. **121**, 083901 (2018).
21. S. Ghimire, M. Fuchs, J. Hastings, S. C. Herrmann, Y. Inubushi, J. Pines, S. Shwartz, M. Yabashi, and D. A. Reis, "Nonsequential two-photon absorption from the K shell in solid zirconium," Phys. Rev. A **94**, 043418 (2016).
22. E. Shwartz and S. Shwartz, "Difference-frequency generation of optical radiation from two-color x-ray pulses," Opt. Express **23**, 7471–7480 (2015).
23. E. Allaria, R. Appio, L. Badano, W. A. Barletta, S. Bassanese, S. G. Biedron, A. Borga, E. Busetto, D. Castronovo, P. Cinquegrana, S. Cleva, D. Cocco, M. Cornacchia, P. Craievich, I. Cudin, G. D'Auria, M. Dal Forno, M. B. Danailov, R. De Monte, G. De Ninno, P. Delgiusto, A. Demidovich, S. Di Mitri, B. Diviacco, A. Fabris, R. Fabris, W. Fawley, M. Ferianis, E. Ferrari, S. Ferry, L. Froehlich, P. Furlan, G. Gaio, F. Gelmetti, L. Giannessi, M. Giannini, R. Gobessi, R. Ivanov, E. Karantzoulis, M. Lonza, A. Lutman, B. Mahieu, M. Milloch, S. V. Milton, M. Musardo, I. Nikolov, S. Noe, F. Parmigiani, G. Penco, M. Petronio, L. Pivetta, M. Predonzani, F. Rossi, L. Rumiz, A. Salom, C. Scafuri, C. Serpico, P. Sigalotti, S. Spampinati, C. Spezzani, M. Svandrlik, C. Svetina, S. Tazzari, M. Trovo, R. Umer, A. Vascotto, M. Veronese, R. Visintini, M. Zaccaria, D. Zangrando, and M. Zangrando, "Highly coherent and stable pulses from the FERMI seeded free-electron laser in the extreme ultraviolet," Nat. Photonics **6**, 699–704 (2012).
24. C. Bostedt, J. D. Bozek, P. H. Bucksbaum, R. N. Coffee, J. B. Hastings, Z. Huang, R. W. Lee, S. Schorb, J. N. Corlett, P. Denes, P. Emma, R. W. Falcone, R. W. Schoenlein, G. Doumy, E. P. Kanter, B. Kraessig, S. Southworth, L. Young, L. Fang, M. Hoener, N. Berrah, C. Roedig, and L. F. DiMauro, "Ultra-fast and ultra-intense x-ray sciences: first results from the Linac coherent light source free-electron laser," J. Phys. B **46**, 164003 (2013).

25. D. J. Dunning, B. W. J. McNeil, and N. R. Thompson, "Towards zepto-second-scale pulses from x-ray free-electron lasers," Phys. Procedia **52**, 62–67 (2014).
26. Y. R. Shen, *The Principles of Nonlinear Optics*, Wiley Classics Library (Wiley-Interscience, 2003).
27. S. Shwartz and S. E. Harris, "Polarization entangled photons at x-ray energies," Phys. Rev. Lett. **106**, 080501 (2011).
28. A. Schori, C. Bömer, D. Borodin, S. P. Collins, B. Detlefs, M. Moretti Sala, S. Yudovich, and S. Shwartz, "Parametric down-conversion of x rays into the optical regime," Phys. Rev. Lett. **119**, 253902 (2017).
29. H. R. Phillip and E. A. Taft, "Kramers-Kronig analysis of reflectance data for diamond," Phys. Rev. **136**, A1445–A1448 (1964).
30. "Atomic scattering factors," http://henke.lbl.gov/optical_constants/asf.html.
31. G. D. Boyd and D. A. Kleinman, "Parametric interaction of focused Gaussian light beams," J. Appl. Phys. **39**, 3597–3639 (1968).
32. H. Wang and A. M. Weiner, "Efficiency of short-pulse type-I second-harmonic generation with simultaneous spatial walk-off, temporal walk-off, and pump depletion," IEEE J. Quantum Electron. **39**, 1600–1618 (2003).
33. S. Yudovich and S. Shwartz, "Second-harmonic generation of focused ultrashort x-ray pulses," J. Opt. Soc. Am. B **32**, 1894–1900 (2015).
34. S. D. Shastri, P. Zambianchi, and D. M. Mills, "Dynamical diffraction of ultrashort x-ray free-electron laser pulses," J. Synchrotron Radiat. **8**, 1131–1135 (2001).
35. T. Osaka, T. Hirano, Y. Sano, Y. Inubushi, S. Matsuyama, K. Tono, T. Ishikawa, K. Yamauchi, and M. Yabashi, "Wavelength-tunable split-and-delay optical system for hard x-ray free-electron lasers," Opt. Express **24**, 9187–9201 (2016).
36. W. Lu, T. Noll, T. Roth, I. Agapov, G. Geloni, M. Holler, J. Hallmann, G. Ansaldi, S. Eisebitt, and A. Madsen, "Design and throughput simulations of a hard x-ray split and delay line for the MID station at the European XFEL," in *12th International Conference on Synchrotron Radiation Instrumentation* (2016), paper 030010.
37. S. P. Hau-Riege, R. M. Bionta, D. D. Ryutov, and J. Krzywinski, "Measurement of x-ray free-electron-laser pulse energies by photoluminescence in nitrogen gas," J. Appl. Phys. **103**, 053306 (2008).
38. K. Tiedtke, J. Feldhaus, U. Hahn, U. Jastrow, T. Nunez, T. Tschentscher, S. V. Bobashev, A. A. Sorokin, J. B. Hastings, S. Möller, L. Cibik, A. Gottwald, A. Hoehl, U. Kroth, M. Krumrey, H. Schöppe, G. Ulm, and M. Richter, "Gas detectors for x-ray lasers," J. Appl. Phys. **103**, 094511 (2008).
39. S. Moeller, J. Arthur, A. Brachmann, R. Coffee, F.-J. Decker, Y. Ding, D. Dowell, S. Edstrom, P. Emma, Y. Feng, A. Fisher, J. Frisch, J. Galayda, S. Gilevich, J. Hastings, G. Hays, P. Hering, Z. Huang, R. Iverson, J. Krzywinski, S. Lewis, H. Loos, M. Messerschmidt, A. Miahnahri, H.-D. Nuhn, D. Ratner, J. Rzepiela, D. Schultz, T. Smith, P. Stefan, H. Tompkins, J. Turner, J. Welch, B. White, J. Wu, G. Yocky, R. Bionta, E. Ables, B. Abraham, C. Gardener, K. Fong, S. Friedrich, S. Hau-Riege, K. Kishiyama, T. McCarville, D. McMahon, M. McKernan, L. Ott, M. Pivovaroff, J. Robinson, D. Ryutov, S. Shen, R. Soufli, and G. Pile, "Photon beamlines and diagnostics at LCLS," Nucl. Instrum. Methods Phys. Res. A **635**, S6–S11 (2011).
40. "XFEL comparison," https://www.xfel.eu/facility/comparison/index_eng.html.
41. J. F. Schmerge, A. Brachmann, D. A. Dowell, A. Fry, R. K. Li, Z. Li, T. O. Raubenheimer, T. Vecchione, F. Zhou, M. Park, A. Bartnik, I. V. Bazarov, B. M. Dunham, C. Gulliford, C. Mayes, A. Lunin, N. Solyak, A. Vivoli, D. Filippetto, R. Huang, C. Papadopoulos, G. Portmann, J. Qiang, F. Sannibale, S. P. Virostek, and R. Wells, "The LCLS-II injector design," Technical Report SLAC-PUB-16211 (2015).
42. J. Stohr, "Linac coherent light source II (LCLS-II) conceptual design report," Technical Report SLAC-R-978 (2011).
43. A. P. Mancuso, A. Aquila, G. Borchers, K. Giewekemeyer, and N. Reimers, "Technical design report: scientific instrument single particles, clusters, and biomolecules (SPB)," Technical Report XFEL.EU TR-2011-007 1–232 (2013).
44. J. Galayda, "The Linac Coherent Light Source-II Project," in *5th International Particle Accelerator Conference (IPAC)*, Dresden, Germany, June15–20, 2014, pp. 935–937.